nature physics

ARTICLES

PUBLISHED ONLINE: 6 JANUARY 2013 | DOI: 10.1038/NPHYS2515

The role of non-equilibrium vibrational structures in electronic coherence and recoherence in pigment–protein complexes

A. W. Chin[1,2], J. Prior[3], R. Rosenbach[1], F. Caycedo-Soler[1], S. F. Huelga[1] and M. B. Plenio[1]*

Recent observations of oscillatory features in the optical response of photosynthetic complexes have revealed evidence for surprisingly long-lasting electronic coherences which can coexist with energy transport. These observations have ignited multidisciplinary interest in the role of quantum effects in biological systems, including the fundamental question of how electronic coherence can survive in biological surroundings. Here we show that the non-trivial spectral structures of protein fluctuations can generate non-equilibrium processes that lead to the spontaneous creation and sustenance of electronic coherence, even at physiological temperatures. Developing new advanced simulation tools to treat these effects, we provide a firm microscopic basis to successfully reproduce the experimentally observed coherence times in the Fenna–Matthews–Olson complex, and illustrate how detailed quantum modelling and simulation can shed further light on a wide range of other non-equilibrium processes which may be important in different photosynthetic systems.

Photosynthesis is a fundamental biological process which provides the primary source of energy for almost all terrestrial life[1]. In its early stages, ambient photons are absorbed by optically active molecules (pigments) in an antenna complex, leading to the formation of molecular excited states (excitons). These then migrate by excitation energy transfer (EET) through pigment–protein complexes (PPCs) to a reaction centre where the exciton's energy is used to release an electron— Fig. 1. Remarkably, these processes often have a quantum efficiency of almost 100% (refs 1,2), and uncovering the underlying biological design principles could inspire important new developments in artificial light-harvesting technologies[3]. The potential novelty of a biomimetic approach to light-harvesting is underlined by the unexpected observation of robust, long-lasting oscillatory features in two-dimensional spectra of PPCs extracted from bacteria, algae and higher plants. Using ultrafast nonlinear spectroscopy, sustained beating between optically excited states lasting several hundreds of femtoseconds at room temperature, and up to nearly 2 ps in the Fenna–Matthews–Olson (FMO) complex at 77 K, have been observed[4–8]. These experiments have been interpreted as evidence for electronic coherences between excitons, with lifetimes which are, surprisingly, over an order of magnitude larger than coherences between electronic ground and excited states[7]. Such coherence times are long enough for EET and excitonic coherence to coexist, conditions under which a sophisticated interplay of quantum and dissipative processes theoretically optimizes transport efficiency[9–12].

Although many proposals for how quantum effects might enhance biological light-harvesting have been advanced over the past five years, most of these have used simple, phenomenological methods to include decoherence[9–13]. In this article we tackle the more fundamental problem of elucidating the microscopic mechanisms through which the wide range of electronic coherence times observed in PPCs actually arise. By including the full temperature dependence into the numerically exact Time Evolving Density with Orthogonal Polynomial Algorithm (TEDOPA) of refs 14–16, we show that the presence of resonant structure in the spectral function of PPC chromophores leads to non-equilibrium quantum dynamics in which picosecond electronic coherence can be driven and supported by quasicoherent interactions between excitons and spectrally sharp vibrational environment modes[17–20]. Moreover, both the decay of ground–excited state coherences and the excitation energy transport exhibit the correct timescales, thus explaining three crucial observations within the same model. We complement our numerics with an approximate semi-classical model that illustrates the essential physical mechanisms by which discrete modes, driven far from equilibrium by exciton injection, may spontaneously generate and sustain oscillatory EET and electronic coherence against aggressive background decoherence, and that also helps to isolate the roles of other processes, such as non-Markovian pure dephasing[21,22]. Under these conditions, energy transport proceeds in a non-equilibrium fashion, transiently violating the detailed balance conditions which are often invoked to set fundamental limits on light-harvesting efficiency[23]. The requirements for observing this striking behaviour in ensemble experiments are discussed in Supplementary Section SC.

The physics of vibration-induced coherence

The electronic Hamiltonian of a PPC consists of a network of chromophoric sites, denoted $|i\rangle$, each supporting a single optical excitation of energy ϵ_i, which can transfer coherently onto another site j with a (dipolar) interaction amplitude J_{ij}. Each excitation is also linearly coupled to its local environmental fluctuations, which are modelled as independent continua of harmonic vibrational modes[9,10], as detailed in Supplementary Section SA1. Denoting the exciton eigenstate of energy E_n as $|e_n\rangle = \sum_i C_i^n |i\rangle$ and ω_k as the vibrational modes of the protein, the full Hamiltonian of the

[1]Institute of Theoretical Physics, Universität Ulm, Albert-Einstein-Allee 11, 89069 Ulm, Germany, [2]Theory of Condensed Matter Group, Cavendish Laboratory, University of Cambridge, J J Thomson Avenue, Cambridge, CB3 0HE, UK, [3]Departamento de Física Aplicada, Universidad Politécnica de Cartagena, Cartagena 30202, Spain. *e-mail: martin.plenio@uni-ulm.de.

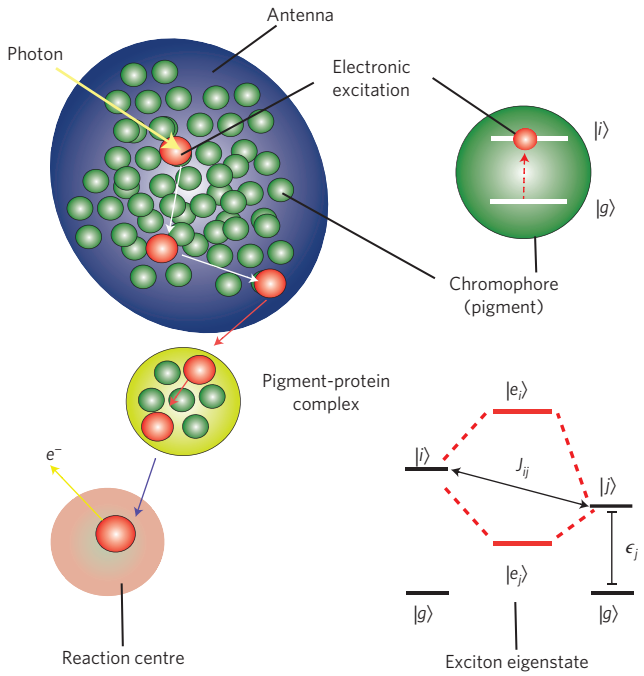

Figure 1 | The generic organization of the early stages of light-harvesting in natural photosynthesis. Excitons created in the antenna complexes migrate via dipolar coupling between chromophores in different pigment–protein complexes and are finally transferred to a reaction centre where charge separation occurs. Under the low-light conditions where light-harvesting is most efficient, most of the intermediate pigment–protein complexes transport only single excitons at a time and each complex functions independently. Chromophores are modelled as having a ground state $|g\rangle$ and an optically excited state $|i\rangle$. Couplings between chromophores leads to the formation of delocalized excitonic eigenstates $|e_i\rangle$, with transitions between these states mediated by environmental fluctuations.

exciton–protein system can be be written as $H = H_{ex} + H_I + H_B$, where $H_{ex} = \sum_n E_n |e_n\rangle\langle e_n|$, $H_B = \sum_{ik} \omega_k a_{ik}^\dagger a_{ik}$ and

$$H_I = \frac{1}{2}\sum_{n,m} (Q_{nm}|e_n\rangle\langle e_m| + \text{h.c.}) \quad (1)$$

$$Q_{nm} = \sum_{ik} \sqrt{S_{ik}}\omega_k C_n^i C_m^i (a_{ik} + a_{ik}^\dagger) \quad (2)$$

Operators $a_{ik}, a_{ik}^\dagger$ denote bosonic destruction and creation operators for the kth independent vibrational mode coupled to site i. The exciton-mode interactions are set by their Huang-Rhys factors S_{ik} (ref. 18). Finally, we assume, for simplicity only, identical, independent vibrational environments on each site characterized by a spectral density $J(\omega) = \sum_k S_{ik}\omega_k^2 \delta(\omega - \omega_k)$. The key findings presented here arise from our consideration of structured spectral functions which contain two contributions; a smooth background describing fluctuations, probably due to the protein environment, and also couplings to discrete vibrational modes, which may be of intramolecular origin.

From equations (1) and (2), we see that the exciton–environment interaction contains transverse (non-adiabatic) terms which couple different excitonic states through the bath displacement operators. Neglecting non-Markovian effects, the strongly-damped response of the background environment drives incoherent exciton relaxation through these terms[18]. However, coupling to sharp (underdamped), quasi-resonant discrete modes allows the possibility of coherent and reversible inter-exciton transitions through the long-lasting mechanical (coherent) motion of the mode displacements. From equations (1) and (2), the initial (fast) injection of an exciton, either coherently or incoherently, creates a sudden force on the discrete modes that initiates transient oscillations at approximately their natural frequency ω_k. To first order, these transients can be treated as coherent oscillations and their back action on the excitons then acts essentially like a time-dependent field that drives coherent, Rabi-like transitions between dissipative exciton states via the Hamiltonian terms

$$H_{\text{driving}} \approx \frac{1}{2}\sum_{n\neq m} (\langle Q_{nm}\rangle(t)|e_n\rangle\langle e_m| + \text{h.c.})$$

where $\langle Q_{nm}\rangle(t) \propto \sum_{ik} \sqrt{S_k}\omega_k C_n^i C_m^i \sin(\omega_k t)$. Heuristically, this non-equilibrium, laser-like driving essentially generates new electronic coherences in the system to replace those that are continuously damped out by the fluctuations of the smooth background environment. The actual (coupled) motion of the excitons and modes is more complex, and may also interact with non-Markovian dynamics of the background, but the physical picture presented here illustrates a key point: electronic coherence may emerge from transiently exciting robust, weakly dephasing vibrational coherences which are then used to later transfer coherence back to the excitons, a novel type of coherence generation and storage (see refs 24–29 for related observations that non-equilibrium systems may generate or maintain quantum entanglement).

We should stress that this (re)generating of electronic coherence is a very different concept from protection of coherences by spatial correlations, non-Markovianity, or intrinsically weak environmental dephasing[12,21,22,30]. Crucially, mode-driven coherences will be prominent whenever vibrational modes have frequencies comparable to exciton energy differences of strongly coupled chromophores and have dephasing times on picosecond timescales. Many examples of such modes have been observed experimentally in PPCs, such as the FMO complex[17–20], but their importance as elements in designing efficient transport structures—such as the recently proposed 'phonon antenna'[31]—and for interpreting experimental observations in multidimensional spectroscopy has only just begun to be appreciated[14,32,33]. This mechanism, based on resonant driving of inter-exciton transitions, will not regenerate or sustain ground to excited state coherence, as the environment does not couple these states. This framework provides a natural understanding of the distinct coherence timescales in the problem which may also be of relevance for photosynthetic charge transfer dynamics[34].

Semiclassical models

To illustrate the physical mechanism of coherence regeneration through coherent (deterministic) motion of discrete modes in excitonic dynamics, we now present semiclassical simulations obtained by treating the coordinates and momenta of the discrete vibrations classically. Full details of how the quantum problem is reduced to a semiclassical description are given in Supplementary Section SB. In the following simulations, interactions with a classical mode of frequency 180 cm^{-1} and $S_k = 0.22$ were included and the spectral function of Adolphs and Renger (AR) used for the background bath[35]—see Supplementary Section SA3. The mode parameters and dephasing rate (1 ps^{-1}) are taken from hole-burning or estimated from fluorescence line-narrowing experiments, as is the background spectral function[17,18,35]. The background bath and modes are initially in thermal equilibrium at temperature T, the background reorganization energy is $\lambda = 35\ \text{cm}^{-1}$ and the seven-chromophore FMO Hamiltonian of *Chlorobium tepidum* was taken from ref. 35. We denote the matrix elements $\langle e_n|\rho(t)|e_m\rangle = \rho_{e_n e_m}(t)$.

Figure 2a shows results at $T = 77$ K. Motivated by current experimental data[5], which focuses on the two lowest exciton states, we present in Fig. 2b the coherences $\mathrm{Re}(\rho_{e_1e_2}(t))$ between exciton states $|e_1\rangle$ and $|e_2\rangle$ with a symmetric superposition of these as the initial state to resemble the laboratory condition after excitation with multiple laser pulses. In the presence of the 180 cm^{-1} modes, which are nearly resonant with $E_1 - E_2 = 150$ cm^{-1}, after a transient behaviour in the first 250 fs the coherence exhibits prominent oscillations with an effective coherence time of ≈950 fs. This is consistent with the coherence times of beating signals seen in FMO experiments[5]. In contrast, for the same background spectral density, but neglecting the 180 cm^{-1} mode, oscillations decay with a coherence time of just 280 fs when measured after a transient period of 250 fs. A multi-frequency beating pattern in the oscillations is apparent in the presence of resonant modes until about 850 fs. This is caused by the beating and dynamical coupling between the electronic coherence initially prepared by the laser excitation and the coherence induced later by the discrete mode motion. The vanishing of this pattern at the same rate as the exciton coherence in the background-only simulation provides direct evidence that initial coherences are not protected but replaced by mode interactions at later times. Both results also show a fast, time-dependent pure dephasing component at early times due to the background environment, described in detail in Supplementary Section SB.

Figure 2b also shows the absolute value of the coherence between $|e_{1,2}\rangle$ and the optical ground state $|g\rangle$, starting from a symmetric superposition of $|e_{1,2}\rangle$ and $|g\rangle$ which closely resembles the evolution probed through accumulated photon echo experiments[36] and recently developed single molecule femtosecond pulse shaping techniques[37]. An additional, faster component to the coherence decay is seen for both coherences at early times when the 180 cm^{-1} mode is included, but the dynamics are qualitatively similar to the background-only case. The residual, slowly decaying component of ρ_{e_1g} is due to the relatively long (≈2.4 ps) lifetime of the lowest energy state at $T = 77$ K and the absence of pure dephasing in the long-time limit in the AR spectral function in the Markov approximation—see Supplementary Section SB1.

Figure 2c,d shows corresponding results at $T = 277$ K. Coherent oscillations lasting up to at least 600 fs have been observed in FMO (refs 5) at this near-ambient temperature. Here we find that the mode interactions lengthen the effective coherence time relative to the background-only simulations even more dramatically, with mode-induced coherence lasting up to 800 fs, compared with just 200 fs in the absence of the mode. The $\rho_{e_{1,2}g}$ coherences all decay with similar, monoexponential time constants in the range 80–100 fs, which are dominated by the short (and almost equal) lifetimes and the transient pure dephasing rates of the exciton state populations at $T = 277$ K—see Supplementary Section SB1.

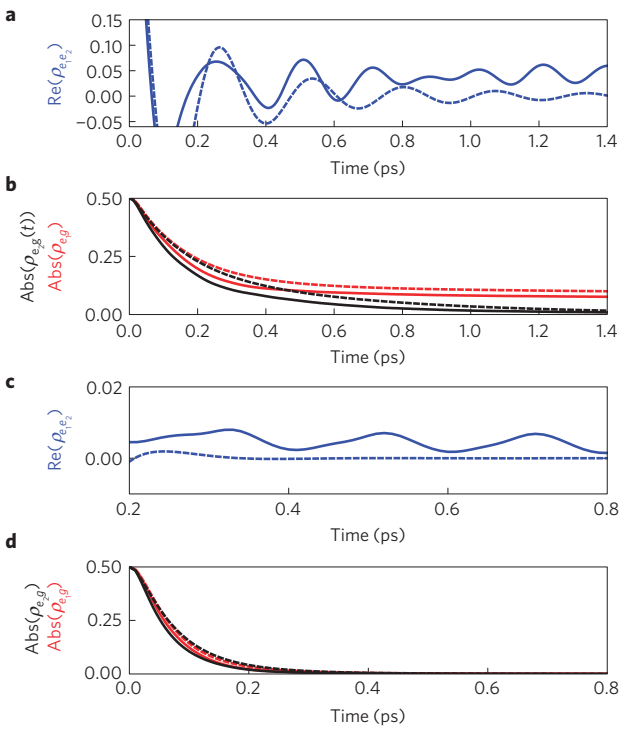

Figure 2 | Electronic coherence from the semiclassical model. a,**b**, Results at $T = 77$ K. **a**, Inter-exciton coherence $\mathrm{Re}(\rho_{e_1e_2}(t))$ for an initial exciton state $2\rho(0) = |e_1\rangle\langle e_1| + |e_2\rangle\langle e_2| + |e_1\rangle\langle e_2| + |e_2\rangle\langle e_1|$. **b**, Ground-excited coherences $\mathrm{Abs}(\rho_{e_1g}(t))$ (in red) and $\mathrm{Abs}(\rho_{e_2g}(t))$ (in black) for an initial exciton state $2\rho(0) = |e_i\rangle\langle e_i| + |g\rangle\langle g| + |e_i\rangle\langle g| + |g\rangle\langle e_i|$ $(i = 1, 2)$, respectively. Note that the optical high-frequency oscillations of the $\rho_{e_ig}(t)$ coherences have been suppressed by taking the absolute value. Exciton population dynamics following the injection of an excitation on site 1 of the FMO complex were also computed at this temperature, showing that excitons relax to the lowest energy states localized around sites 3 and 4 after ≈3 ps (not shown). This is in line with the experimental transport times of several picoseconds[35]. **c**,**d**, Semiclassical results at $T = 277$ K. The same quantities and initial conditions as **a**,**b** are plotted and used in **c**,**d**, respectively. The results at $T = 277$ K in **c**,**d** are plotted on the interval [0.2,0.8] ps to highlight the long lived coherences in the presence of the resonant 180 cm^{-1} mode on a timescale relevant for experiments at this temperature. In all the plots, results including and excluding the resonant 180 cm^{-1} mode are shown as solid and dashed lines, respectively.

Numerically exact simulations

The essentially Markovian treatment presented so far to illustrate the principal physical mechanism responsible for long-lived electronic coherences represents an approximation whose validity must be assessed. Therefore we now present numerically exact results which include all possible effects of discrete mode motion, non-adiabatic coupling and fluctuations, as well as the non-Markovian background. For clarity the new physics are presented for a dimer PPC, an important component of a range of natural PPCs[5,8,38]. We again consider the same background spectral density $J(\omega)$ and 180 cm^{-1} discrete mode of AR (ref. 35). A 37 cm^{-1} mode (with $S_k = 0.1$) which has recently been used to describe features of two-dimensional FMO spectra is also included[32], with parameters taken from fluorescence line-narrowing experiments[18]. The electronic parameters used in the simulations are $J_{12} = 53.5$ cm^{-1}, $\epsilon_1 - \epsilon_2 = 130$ cm^{-1}. This gives two exciton eigenstates with an energy difference of 170 cm^{-1}, which is based on sites 3 and 4 of the FMO Hamiltonian[35], and which are fairly typical values for exciton pairs in PPCs[4–6,35]. The evolution of the global system-environment density matrix is then computed using a new finite-temperature extension of the numerically exact TEDOPA method[14–16]—see Supplementary Section SA4. In all simulations the initial state is a product of an exciton state and a thermal state of the environment (which includes the discrete modes). To show that the main effects arise from the presence of the resonant 180 cm^{-1} mode, simulations are carried out both with and without this mode, whilst the non-resonant 37 cm^{-1} mode is always retained.

Inter-exciton and ground–exciton coherences

Figure 3a shows the evolution of the electronic coherence $\rho_{e_1e_2}(t)$ starting from an initially prepared (pure) symmetric superposition of the exciton states $|e_1\rangle$ and $|e_2\rangle$ at $T = 77$ K. With coupling to the 180 cm^{-1} mode, the multi-frequency beating and revival dynamics in the oscillating coherence are again seen, indicating mode-driven coherence. This leads to coherence oscillations with a fast initial dephasing time (200 fs) and a residual, longer-lasting

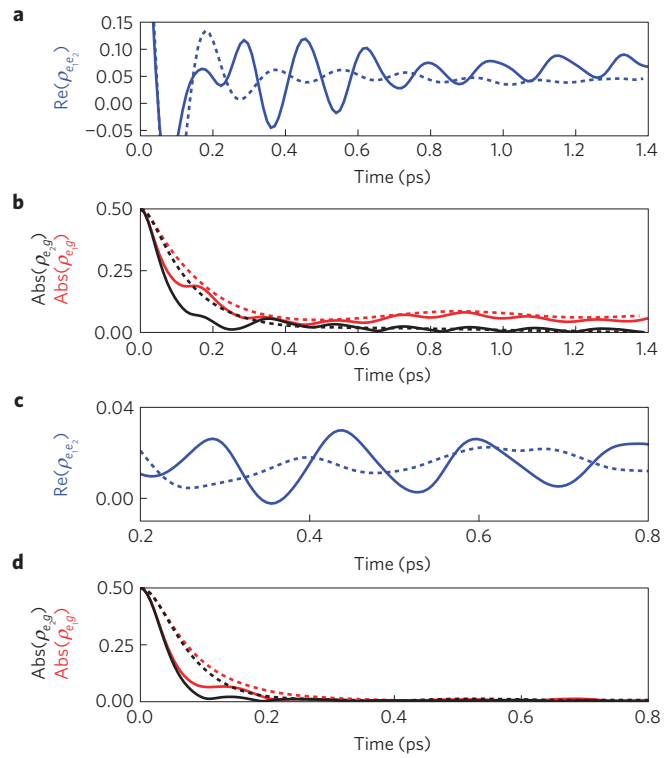

Figure 3 | Numerical exact results of electronic coherence for cryogenic and physiological temperatures. a,**b**, TEDOPA results at $T = 77$ K. **a**, Inter-exciton coherence $\mathrm{Re}(\rho_{e_1e_2}(t))$ for an initial exciton state $2\rho(0) = |e_1\rangle\langle e_1| + |e_2\rangle\langle e_2| + |e_1\rangle\langle e_2| + |e_2\rangle\langle e_1|$. **b**, Ground-excited coherences $\mathrm{Abs}(\rho_{e_1g}(t))$ (in red) and $\mathrm{Abs}(\rho_{e_2g}(t))$ (in black) for an initial exciton state $2\rho(0) = |e_i\rangle\langle e_i| + |g\rangle\langle g| + |e_i\rangle\langle g| + |g\rangle\langle e_i| (i = 1, 2)$, respectively. Note that the optical high-frequency oscillations of the $\rho_{e_ig}(t)$ coherences have been suppressed by taking the absolute value. Weak revivals of $\mathrm{Abs}(\rho_{e_2g}(t))$ (on top of faster amplitude modulations) in the interval [0.3, 0.6] ps arise from coherent population transfer (against the energy gradient) and match similar features seen in Fig. 4a. **c**,**d**, TEDOPA results at $T = 277$ K. The same quantities and initial conditions as **a**,**b** are plotted and used in **c**,**d**, respectively. The results at $T = 277$ K in **c**,**d** are plotted on the interval [0.2, 0.8] ps to highlight the long lived coherences in the presence of the resonant 180 cm^{-1} mode on a timescale relevant for experiments at this temperature. In all the plots, results including and excluding the resonant 180 cm^{-1} mode are shown as solid and dashed lines, respectively.

component arising from mode driving. Similar revival patterns have been observed in time-resolved spectra of FMO[7,32]. At $T = 277\,K$, shown in Fig. 3c, the resonant mode also greatly enhances coherent oscillations relative to the background-only coherences over the first 800 fs, which is, again, consistent with experimental results[5]. The non-resonant mode at 37 cm^{-1} plays no significant role in these inter-exciton dynamics, as expected.

Figure 3b shows the absolute value of the ground–excited state coherences $\rho_{e_ng}(t)$ at $T = 77$ K for initial symmetric superpositions of states $|e_n\rangle$ and $|g\rangle$. The thermal and quantum fluctuations of both the 180 cm^{-1} and 37 cm^{-1} modes induce amplitude modulations of these coherences at the mode frequencies[32], leading to an effectively faster and oscillatory initial decay, followed by slow oscillations on top of the decaying amplitudes. The short effective time constants for all curves lie in the range 150–200 fs, which are consistent with experimental results[7], and faster than those found in the semiclassical approach. The coherence $\rho_{e_2g}(t)$ decays through population relaxation from $|e_2\rangle$ to $|e_1\rangle$; however, on top of the periodic modulation caused by modes, additional weak recurrence features result from oscillatory population transfer induced by

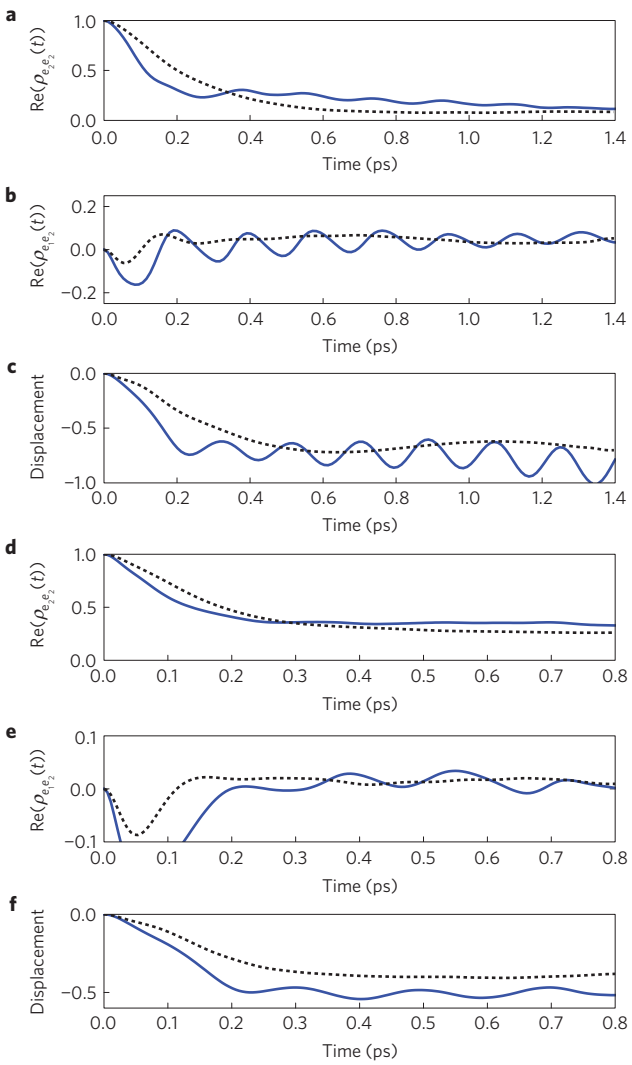

Figure 4 | Spontaneous generation of excitonic coherence. a, Population dynamics, showing $\rho_{e_2e_2}(t)$ for the electronic and mode parameters given in the text. The initial state was $\rho(0) = |e_2\rangle\langle e_2|$ and the environment was at $T = 77$ K. Weak, oscillatory revival of population in the $|e_2\rangle$ state between 0.3 and 0.6 ps matches the revival dynamics of ρ_{e_2g} in Fig. 3b, indicating coherent population (and coherence) transfer. **b**, Spontaneous electronic coherences $Re(\rho_{e_1e_2}(t))$ for same parameters and initial conditions. **c**, Average displacement $\langle X_1\rangle(t)$ for same parameters and initial conditions. **d**–**f**. The same as for **a**–**c**, respectively, but with the environment initially at $T = 277$ K. In all the plots, results including and excluding the resonant 180 cm^{-1} mode are shown as solid and dashed lines, respectively.

the 180 cm^{-1} mode— Fig. 4. The coherence $\rho_{e_1g}(t)$ shows a fast, incomplete and non-Markovian decay (≈150 fs) initially, followed by an extremely slow decay due to the long-time absence of pure dephasing in the AR (super-ohmic) spectral density and the long (≈2.4 ps) lifetime of the lowest energy excited state $|e_1\rangle$ at $T = 77$ K. Long $|e_1\rangle\langle g|$ coherence times (10–100 ps) have been seen in previous FMO photon echo measurements at low temperatures ($T < 50$ K; ref. 36). At $T = 277$ K (Fig. 3d), both ground to excited state coherences decay rapidly owing to the fast population relaxation to thermal equilibrium and enhanced pure dephasing. Again, the additional oscillatory decay in the presence of the resonant modes in the TEDOPA simulations leads to significantly faster reduction of coherence (with time constant of 50 fs) compared to the semiclassical approach which neglects the quantum fluctuations of the environment.

Population oscillations and environmental variables

For $T = 77$ K, Fig. 4a shows the population remaining in $|e_2\rangle$ for the initial state $\rho(0) = |e_2\rangle\langle e_2|$, which does not contain any initial inter-exciton coherence and may be created by incoherent excitation alone. The presence of the 180 cm^{-1} mode induces population oscillations in the population decay, which explain the similar oscillations seen in $\rho_{e_1 g}(t)$ in Fig. 3b, and is also direct evidence of weak coherence transfer (not shown). Population oscillations have also recently been observed in FMO[39], and imply a partially reversible energy exchange with the environment that transiently violates detailed balance. Figure 4b shows the spontaneous generation of oscillatory coherences over these population dynamics. Non-Markovian effects (finite reorganization time) and the 37 cm^{-1} mode are also seen to generate short-lived spontaneous coherences; however, these are transient and only the 180 cm^{-1} mode drives strong long-lasting coherence oscillations. No spontaneous coherence arises in the standard Bloch–Redfield description, showing the essential need to go beyond such theories—see Supplementary Section SB1. In Fig. 4c, we make use of the complete environment information provided by TEDOPA to show the expectation value of the collective environment coordinate X_1. Fig. 4c shows that the exciton-mode interaction leads to long-lasting coherent environmental oscillations which drive exciton transitions, confirming the semiclassical picture and coherence-generating mechanism previously outlined. In the absence of resonant modes, these strong oscillatory features vanish in the collective mode and exciton populations. Figure 4d–f shows that, remarkably, the same non-equilibrium and spontaneously coherent dynamics are also present (though less strong) at $T = 277$ K.

We finally observe that the spontaneous coherence in Fig. 4b tends to a (small), non-oscillating, non-zero value at long times at $T = 77$ K, indicating that the exciton-mode steady states generated by the dynamics are quantum superpositions of excitonic and vibrational degrees of freedom. Indeed, the prolonged coherent dynamics leading to these steady states could also be looked at in terms of the dynamical hybridization (formation of superposition states) which quantum mechanically mixes exciton and (weakly damped) discrete vibrational states. At $T = 277$ K these transient states lead to longer-lasting oscillatory coherence, but the strong dephasing of the background fluctuations prevents these states from being stable in equilibrium. Other examples of how mode interactions may alter the relaxed electronic states are given in Supplementary Section SD, which sets out how discrete modes may provide an insight into anomalous oscillations recently observed in conjugated polymers[40,41].

Our results show that PPCs—as exemplified by FMO—provide a situation outside of the standard open quantum system paradigm where non-equilibrium processes can compete with the purely dissipative action of the thermal background. The real-time correlations in the exciton–environment state that emerge in this scenario have not yet been explored in great detail, and methods such as TEDOPA could be used to look at this new problem in other PPC structures where such conditions could be important and might also drive new, potentially efficient, dynamical phenomena. The experimental verification of the dynamics discussed in this work would provide further ground for the consolidation of quantum biology as a new, truly multidisciplinary research field with significant implications for the fundamental physics at the border of the quantum and classical domains.

Received 19 March 2012; accepted 20 November 2012; published online 6 January 2013

References

1. Blankenship, R. *Molecular Mechanisms of Photosynthesis* (Wiley-Blackwell, 2002).
2. Van Amerongen, H., Valkunas, L. & van Grondelle, R. *Photosynthetic Excitons* (World Scientific, 2000).
3. Scholes, G., Fleming, G., Olaya-Castro, A. & van Grondelle, R. Lessons from nature about solar light harvesting. *Nature Chem.* **3,** 763–774 (2011).
4. Engel, G. S. *et al.* Evidence for wavelike energy transfer through quantum coherence in photosynthetic complexes. *Nature* **446,** 782–786 (2007).
5. Panitchayangkoon, G. *et al.* Long-lived quantum coherence in photosynthetic complexes at physiological temperature. *Proc. Natl Acad. Sci. USA* **107,** 12766–12770 (2010).
6. Calhoun, T. *et al.* Quantum coherence enabled determination of the energy landscape in light-harvesting complex II. *J. Phys. Chem. B* **113,** 16291–16295 (2009).
7. Hayes, D. *et al.* Dynamics of electronic dephasing in the Fenna–Matthews–Olson complex. *New J. Phys.* **12,** 065042 (2010).
8. Collini, E. *et al.* Coherently wired light-harvesting in photosynthetic marine algae at ambient temperature. *Nature* **463,** 644–647 (2010).
9. Mohseni, M., Rebentrost, P., Lloyd, S. & Aspuru-Guzik, A. Environment-assisted quantum walks in photosynthetic energy transfer. *J. Chem. Phys.* **129,** 174106 (2008).
10. Plenio, M. B. & Huelga, S. F. Dephasing-assisted transport: Quantum networks and biomolecules. *New J. Phys.* **10,** 113019 (2008).
11. Caruso, F., Chin, A. W., Datta, A., Huelga, S. F. & Plenio, M. B. Highly efficient energy excitation transfer in light-harvesting complexes: The fundamental role of noise-assisted transport. *J. Chem. Phys.* **131,** 105106 (2009).
12. Ishizaki, A., Calhoun, T., Schlau-Cohen, G. & Fleming, G. R. Quantum coherence and its interplay with protein environments in photosynthetic electronic energy transfer. *Phys. Chem. Chem. Phys.* **12,** 7319–7337 (2010).
13. Olaya-Castro, A., Lee, C., Olsen, F. & Johnson, N. Efficiency of energy transfer in a light-harvesting system under quantum coherence. *Phys. Rev. B* **78,** 085115 (2008).
14. Prior, J., Chin, A. W., Huelga, S. F. & Plenio, M. B. Efficient simulation of strong system-environment interactions. *Phys. Rev. Lett.* **105,** 050404 (2010).
15. Chin, A. W., Rivas, A., Huelga, S. F. & Plenio, M. B. Exact mapping between system-reservoir quantum models and semi-infinite discrete chains using orthogonal polynomials. *J. Math. Phys.* **51,** 092109 (2010).
16. Chin, A. W., Huelga, S. F. & Plenio, M. B. Chain representations of open quantum systems and their numerical simulation with time-adapative density matrix renormalisation group methods. *Semiconduct. Semimet.* **85,** 115–143 (2011).
17. Matsuzaki, S., Zazubovich, V., Rätsep, M., Hayes, J. & Small, G. Energy transfer kinetics and low energy vibrational structure of the three lowest energy Qy-states of the Fenna-Matthews-Olson antenna complex. *J. Phys. Chem. B* **104,** 9564–9572 (2000).
18. Wending, M. *et al.* Electron-vibrational coupling in the Fenna-Matthews-Olson complex of Prosthecochloris aestuarii determined by temperature-dependent absorption and fluorescence line-narrowing measurements. *J. Phys. Chem. B* **104,** 5825–5831 (2000).
19. Rätsep, M., Blankenship, R. E. & Small, G. J. Energy transfer and spectral dynamics of the three lowest energy Qy-states of the Fenna-Matthews-Olson antenna complex. *J. Phys. Chem. B* **103,** 5736–5741 (1999).
20. Rätsep, M. & Freiberg, A. Electron–phonon and vibronic couplings in the FMO bacteriochlorophyll a antenna complex studied by difference fluorescence line narrowing. *J. Lumin.* **127,** 251–259 (2007).
21. Pachón, P. A. & Brumer, P. The physical basis for long-lived electronic coherence in photosynthetic light harvesting systems. *J. Phys. Chem. Lett.* **2,** 2728–2732 (2011).
22. Kreisbeck, C. & Kramer, T. Long-lived electronic coherence in dissipative exciton-dynamics of light-harvesting complexes. *J. Phys. Chem. Lett.* **3,** 2828–2833 (2012).
23. Scully, M. O., Chaplin, K. R., Dorfman, E., Kim, M. B. & Svidzinsky, A. Quantum heat engine power can be increased by noise-induced coherence. *Proc. Natl Acad. Sci. USA* **108,** 15097–15100 (2011).
24. Plenio, M. B. & Huelga, S. F. Entangled light from white noise. *Phys. Rev. Lett.* **88,** 197901 (2002).
25. Eisert, J., Plenio, M. B., Bose, S. & Hartley, J. Towards quantum entanglement in nanoelectromechanical devices. *Phys. Rev. Lett.* **93,** 190402 (2004).
26. Huelga, S. F. & Plenio, M. B. Stochastic resonance phenomena in quantum many-body systems. *Phys. Rev. Lett.* **98,** 170601 (2007).
27. Hartmann, L., Dür, W. & Briegel, H-J. Entanglement and its dynamics in open, dissipative systems. *New J. Phys.* **9,** 230 (2007).
28. Cai, J. M., Briegel, H. J. & Popescu, S. Dynamic entanglement in oscillating molecules and potential biological implications. *Phys. Rev. E* **82,** 021921 (2010).
29. Semião, F. L., Furuya, K. & Milburn, G. J. Vibration-enhanced quantum transport. *New J. Phys.* **12,** 083033 (2010).
30. Sarovar, M., Cheng, Y. & Whaley, K. Environmental correlation effects on excitation energy transfer in photosynthetic light harvesting. *Phys. Rev. E* **83,** 011906 (2011).

31. Chin, A. W., Huelga, S. F. & Plenio, M. B. Coherence and decoherence in biological systems: Principles of noise-assisted transport and the origin of long-lived coherences. *Phil. Trans. Act. R. Soc. A* **370,** 3638–3657 (2012).
32. Caycedo-Soler, F., Chin, A. W., Almeida, J., Huelga, S. F. & Plenio, M. B. The nature of the low energy band of the Fenna-Matthews-Olson complex: Vibronic signatures. *J. Chem. Phys.* **136,** 155102 (2012).
33. Christensson, N., Kauffmann, H., Pullerits, T. & Mancal, T. Origin of long-lived coherences in light-harvesting complexes. *J. Phys. Chem. B* **116,** 7449–7454 (2012).
34. Novoderezhkin, V. I., Yakovlev, A. G., van Grondelle, R. & Shuvalov, V. A. Coherent nuclear and electronic dynamics in primary charge separation in photosynthetic reaction centers: A redfield theory approach. *J. Chem. Phys. B* **108,** 7445–7457 (2004).
35. Adolphs, J. & Renger, T. How proteins trigger excitation energy transfer in the fmo complex of green sulfur bacteria. *Biophys. J.* **91,** 2778–2797 (2006).
36. Louwve, R. J. W. & Aartsma, T. J. On the nature of energy transfer at low temperatures in the bchl a pigment-protein complex of green sulfur bacteria. *J. Chem. Phys. B* **101,** 7221–7226 (1997).
37. Hildner, R., Brinks, D. & van Hulst, N. Femtosecond coherence and quantum control of single molecules at room temperature. *Nature Phys.* **7,** 172–177 (2010).
38. Theiss, C. *et al.* Pigment-pigment and pigment-protein interactions in recombinant water-soluble chlorophyll proteins (WSCP) from cauliflower. *J. Phys. Chem. B* **111,** 13325–13335 (2007).
39. Panitchayangkoon, G. *et al.* Direct evidence of quantum transport in photosynthetic light-harvesting complexes. *Proc. Natl Acad. Sci. USA* **108,** 20908–20912 (2011).
40. Collini, E. & Scholes, G. Coherent intrachain energy migration in a conjugated polymer at room temperature. *Science* **323,** 369–373 (2009).
41. Collini, E. & Scholes, G. Electronic and vibrational coherences in resonance energy transfer along MEH-PPV chains at room temperature. *J. Phys. Chem. A* **113,** 4223–4241 (2009).

Acknowledgements

This work was supported by the Alexander von Humboldt-Foundation, the EU STREP project PICC and the EU Integrated Project Q-ESSENCE. A.W.C. acknowledges support from the Winton Programme for the Physics of Sustainability. J.P. was supported by Ministerio de Ciencia e Innovación Project No. FIS2009-13483-C02-02 and the Fundación Séneca Project No. 11920/PI/09-j. We acknowledge the bwGRiD project (http://www.bw-grid.de) for the computational resources. Aspects of this work have benefited from discussions with J. Almeida, A. G. Dijkstra, D. Hayes, J. Caram, G. S. Engel and R. van Grondelle.

Author contributions

S.F.H. and M.B.P. designed the research with input from A.W.C.; A.W.C. and F.C-S. carried out the analytical calculations with advice from S.F.H. and M.B.P.; J.P. and R.R. developed the numerical codes and carried out the numerical simulations with guidance from A.W.C. and M.B.P. All authors discussed the results. S.F.H. and M.B.P. led the project. A.W.C., F.C.S., S.F.H. and M.B.P. wrote the manuscript with input of all authors.

Additional information

Supplementary information is available in the online version of the paper. Reprints and permissions information is available online at www.nature.com/reprints. Correspondence and requests for materials should be addressed to M.B.P.

Competing financial interests

The authors declare no competing financial interests.